The mystery of birefringent garnet: is the symmetry lower than cubic?

Sytle M. Antao[a)]
Department of Geoscience, University of Calgary, Calgary, Alberta T2N 1N4, Canada

(Received 23 April 2013; accepted 21 May 2013)

The cause of birefringence in several garnet-group minerals with general chemical formula, $^{[8]}X_3^{[6]}Y_2^{[4]}Z_3^{[4]}O_{12}$, which was observed over 100 years ago, is unknown, although many different reasons were proposed, including symmetry lower than cubic. In this study, electron microprobe analyses (EMPA) were obtained for a Ti-rich andradite, ideally $Ca_3(Fe_2^{3+})Si_3O_{12}$, from Magnet Cove, Arkansas, USA, and the results show that the sample is inhomogeneous with two distinct compositions. The crystal structure was refined by the Rietveld method, cubic space group $Ia\bar{3}d$, and monochromatic synchrotron high-resolution powder X-ray diffraction (HRPXRD) data, which shows a mixture of three distinct cubic phases that are intergrown together and cause birefringence because of strain arising from small structural mismatch. This mixture of three cubic phases was not observed by any other experimental technique. These results have many implications, including garnet phase transitions from cubic to lower symmetry in the mantle, which has important geophysical consequences. © *2013 International Centre for Diffraction Data.* [doi:10.1017/S0885715613000523]

Key words: andradite, birefringence, three-phase intergrowth, Rietveld refinements, synchrotron high-resolution powder X-ray diffraction (HRPXRD), crystal structure

I. INTRODUCTION

Birefringence in garnet was reported over a century ago (Brauns, 1891), but the origin has remained questionable. Several members of the garnet-group minerals are birefringent when viewed under cross-polarized light in a petrographic microscope, hence optically they are not cubic. Many reasons were given as the cause of the birefringence (Ingerson and Barksdale, 1943; Chase and Lefever, 1960; Blanc and Maisonneuve, 1973; Lessing and Standish, 1973; Foord and Mills, 1978; Kitamura and Komatsu, 1978; Takéuchi *et al.*, 1982; Akizuki, 1984; Rossman and Aines, 1986; Allen and Buseck, 1988; Kingma and Downs, 1989; Armbruster *et al.*, 1992; Griffen *et al.*, 1992; Brown and Mason, 1994; Akizuki *et al.*, 1998; Hofmeister *et al.*, 1998; Shtukenberg *et al.*, 2001, 2005; Wildner and Andrut, 2001; Frank-Kamenetskaya *et al.*, 2007), but none of these suggestions provide a unique solution (Allen and Buseck, 1988). This study shows that a mixture of three cubic phases with slightly different structural and chemical parameters occurs together and gives rise to strain arising from structural mismatch and cause anisotropy in birefringent garnet samples. This is in contrast to ABO_3 synthetic garnet samples, such as $CaGeO_3$, $CdGeO_3$ (Prewitt and Sleight, 1969), $MnSiO_3$ (Fujino *et al.*, 1986), and $MgSiO_3$ (Angel *et al.*, 1989; Hatch and Ghose, 1989; Parise *et al.*, 1996) that undergo a cubic to tetragonal transition, where the tetragonal phase is birefringent. However, the present results cast some doubt on these observations.

Garnet-group minerals have important physical properties because of dense packing of the constituent atoms (high hardness, high density, high refractive index, etc.). Synthetic rare-earth varieties can have any color in the visible spectrum, and some possess good laser properties (Geusic *et al.*, 1964). In solid-state science, garnet-type materials are important because of their ferrimagnetism and antiferromagnetism (Bertaut and Forrat, 1956; Geller and Gilleo, 1957). Some garnet varieties spontaneously polarize in electric and magnetic fields, hence they cannot be cubic (Geller, 1967). Although the structure of many birefringent garnet samples were refined in non-cubic space groups, this study shows that the structure of a birefringent garnet is cubic and contains an intergrowth of three different cubic phases.

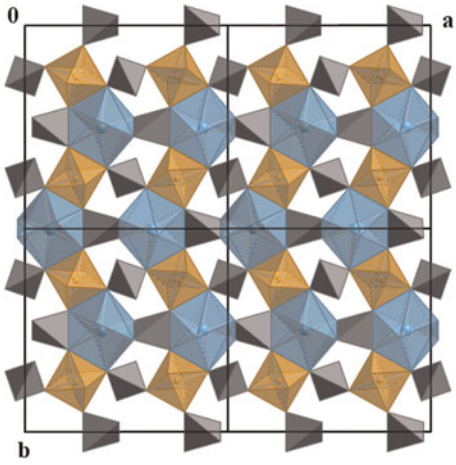

Figure 1. (Color online) Projection of the cubic garnet structure down **c** showing the ZO_4 tetrahedra (gray), YO_6 octahedra (yellow), and XO_8 dodecahedra (blue) that occur as a distorted cubic shape. Dense packing of the polyhedra are obvious from the four unit cells displayed, which shows the prominent edge-sharing and zigzag arrangement of alternating octahedra and dodecahedra.

a) Author to whom correspondence should be addressed. Electronic mail: antao@ucalgary.ca

The cubic crystal structure of garnet with general formula, $^{[8]}X_3^{[6]}Y_2^{[4]}Z_3^{[4]}O_{12}$, consists of alternating ZO_4 tetrahedra and YO_6 octahedra with X atoms filling cavities to form XO_8 dodecahedra. The eight O atoms in the XO_8 polyhedra occur at the corners of a distorted cube (Figure 1). The O atom is bonded to two X, one Y, and one Z in a tetrahedral configuration.

The flexibility of the garnet structure allows it to accommodate the most abundant divalent (X), trivalent (Y), and tetravalent (Z) cations on Earth, and gives rise to the general formula $^{[8]}X_3^{[6]}Y_2^{[4]}Z_3^{[4]}O_{12}$, where the eight-coordinated dodecahedral X site, denoted [8], contains Mg, Ca, Mn^{2+}, or Fe^{2+} cations, the six-coordinated octahedral Y site contains Al, Fe^{3+}, Ti^{4+}, or Zr^{4+} cations, and the four-coordinated tetrahedral Z site contains Si, Fe^{3+} or Al cations, or (F, O_4H_4) groups (Novak and Gibbs, 1971; Smyth *et al.*, 1990; Armbruster *et al.*, 1998).

Ti-rich andradite samples are referred to as "melanite", schorlomite, or morimotoite, depending on the Ti content. The substitution mechanisms and their nomenclature were addressed (Chakhmouradian and McCammon, 2005). Two substitution mechanisms occur at the Z site. One type of Si-deficient Ti-rich andradite can be interpreted as a solid solution between andradite, $Ca_3(Fe_2^{3+})Si_3O_{12}$, and the theoretical end-member morimotoite, $Ca_3(Ti^{4+}Fe^{2+})Si_3O_{12}$, together with minor hydroxy substitution $(O_4H_4) \leftrightarrow SiO_4$ (Lager *et al.*, 1989; Armbruster, 1995). The second type of substitution on the Z site is (Fe^{3+}, Al) ↔ Si, and charge balance is achieved with Ti^{4+} on the Y site (Armbruster *et al.*, 1998; Locock, 2008), and gives rise to the theoretical end-member schorlomite, $Ca_3Ti_2^{4+}[Fe_2^{3+}Si]O_{12}$ (Henmi *et al.*, 1995). The exact substitution mechanism is the subject of several controversial debates based mainly on spectroscopic studies (Armbruster *et al.*, 1998).

This study examines the chemical composition and crystal structure of a Ti-rich birefringent andradite sample from Magnet Cove using electron microprobe analysis (EMPA) and synchrotron high-resolution powder X-ray diffraction (HRPXRD) data. The latter technique uses a short wavelength [0.41351(2) Å], superior resolution, and high peak-to-background discrimination. Preliminary reports were presented (Antao *et al.*, 2013a, 2013b).

II. EXPERIMENTAL

A. Electron microprobe analysis (EMPA) and synchrotron high-resolution powder X-ray diffraction (HRPXRD)

The dark-brown Ti-rich andradite sample (MC9) from Magnet Cove, Hot Spring County, Arkansas, USA appears homogeneous in plane-polarized light and is weakly birefringent under cross-polarized light, where it appears as dark gray instead of black. However, some striking examples of birefringent garnets that contain mottled or tweed-like texture, lamellar, oscillatory, or concentric zoning are available in the recent literature (e.g., Badar *et al.*, 2010; Antao and Klincker, 2013; Badar *et al.*, 2013).

A fragment of the sample (≈0.2 mm in diameter) was analyzed with a JEOL JXA-8200 electron microprobe analyzer (EMPA) using the wavelength-dispersive operating conditions of 15 kV accelerating voltage, 20 nA beam current, a beam diameter of 5 μm, and various mineral standards. The EMPA data were obtained from eight spots from different areas of the crystal and reduced to cations (Table I).

HRPXRD data were obtained at beamline 11-BM, Advanced Photon Source (APS), Argonne National Laboratory (ANL). A small (≈0.2 mm in diameter) fragment of the sample was crushed to a fine powder using an agate mortar and pestle, and loaded into a Kapton capillary (0.8-mm internal diameter) and rotated at a rate of 90 rotations per second. The data were collected at 23 °C to a maximum 2θ of about 50° with a step size of 0.001° and a step time of 0.1 s per step. The HRPXRD trace was collected with 12 silicon (111) crystal analyzers. A silicon (NIST 640c) and alumina (NIST 676a) standard (ratio of ⅓ Si : ⅔ Al_2O_3 by weight) was used to calibrate the instrument and refine the monochromatic wavelength (Table II). Additional details of the experimental set-up are given elsewhere (Antao *et al.*, 2008; Lee *et al.*, 2008; Wang *et al.*, 2008).

The HRPXRD data were analyzed by the Rietveld method (Rietveld, 1969) using the *GSAS* program (Larson and Von Dreele, 2000), EXPGUI interface (Toby, 2001), scattering curves for neutral atoms, and a starting structural model from Antao and Klincker (2013). A full-matrix least-squares refinement was carried out by varying a scale factor, cell parameter, atom coordinates, and isotropic displacement parameters. The HRPXRD trace shows three separate cubic phases with slightly different unit-cell parameters (Figure 2). The three cubic phases were refined together with the site occupancy factors (*sofs*) in terms of the dominant atom in the X, Y, and Z sites. At the end of the refinement, all the parameters were varied simultaneously until the refinement converged. The unit-cell parameters and the Rietveld refinement statistics for three cubic phases are listed in Table II. Atom coordinates, isotropic displacement parameters, and *sofs* are given in Table III. Bond distances are given in Table IV.

III. RESULTS AND DISCUSSION

The EMPA results show two phases with slightly different compositions of $\{Ca_{2.96}Mg_{0.01}Mn_{0.03}^{2+}\}_{\Sigma3}[Fe_{1.61}^{3+}Ti_{0.30}^{4+}Mg_{0.08}Al_{0.01}^{3+}Fe_{0.01}^{2+}]_{\Sigma2}(Si_{2.80}Al_{0.21})_{\Sigma3}O_{12}$ (phase-1, 46.5(1) wt% from HRPXRD); and $\{Ca_{2.96}Mg_{0.01}Mn_{0.03}^{2+}\}_{\Sigma3}[Fe_{1.40}^{3+}Ti_{0.46}^{4+}Mg_{0.12}Fe_{0.02}^{2+}]_{\Sigma2}(Si_{2.69}Al_{0.20}Fe_{0.11}^{3+})_{\Sigma3}O_{12}$ [phase-2, 23.9(1) wt%]. Phase-2 (average of four data points) contains more Ti^{4+} and less Fe^{3+} than phase-1 (average of four data points). In the X site, the amount of Ca is quite high (≈2.96 apfu instead of three). In the Y site, Fe^{3+} is the dominant cation followed by Ti^{4+}. The Z site contains some Al and Fe^{3+} in phase-2. Distinct compositions for individual phases are not always observed by EMPA because the intergrowth of distinct cubic phases may occur on a fine scale.

The HRPXRD results clearly show that the Ti-rich andradite sample consists of a mixture of three cubic phases intergrown together, and is observed by splitting of diffraction peaks (Figure 2). Some other samples from Magnet Cove are single phase, cubic, optically isotropic, and contain no split diffraction peaks (unpublished results). The unit-cell parameters for each of the three cubic phases are slightly different from each other and each phase occurs in significant quantity, as shown by their weight percentages (wt%) in Table II.

https://doi.org/10.1017/S0885715613000523 Published online by Cambridge University Press

TABLE I. Electron microprobe analysis[a] for a Ti-rich andradite (MC9).

Oxide (wt%)	MC9a	MC9b	Cations (for 12 O atoms)	MC9b	MC9b
SiO_2	33.37(15)	32.11(26)	Mn^{2+}	0.026(3)	0.028(3)
TiO_2	4.68(14)	7.22(37)	Mg	0.010(5)	0.012(3)
Al_2O_3	2.15(3)	2.03(25)	Ca	2.964(8)	2.960(5)
Cr_2O_3	0.01(1)	0.00(0)	$\sum X$	3.000	3.000
FeO_{tot}	23.05(23)	21.91(26)	Ti^{4+}	0.295(9)	0.455(23)
MnO_{tot}	0.37(3)	0.40(4)	Al	0.007(9)	0.000(0)
MgO	0.74(1)	1.06(13)	Cr^{3+}	0.001(1)	0.000(0)
CaO	33.03(7)	32.99(13)	Fe^{2+}	0.006(11)	0.023(15)
$\sum$	97.40	97.71	Fe^{3+}	1.608(23)	1.401(28)
			Mn^{3+}	0.000(3)	0.000(0)
Recalc. (wt%)			Mg	0.083(5)	0.121(19)
Final FeO	0.09(16)	0.32(21)	$\sum Y$	2.000	2.000
Final Fe_2O_3	25.52(36)	23.99(26)	Si	2.795(10)	2.689(18)
Final MnO	0.37(4)	0.40(4)	Al	0.205(8)	0.200(24)
Final Mn_2O_3	0.00(5)	0.00(0)	Fe^{3+}	0.000(3)	0.111(33)
$\sum$(calc.)	99.96	100.12	$\sum Z$	3.000	3.000
End-member mole %					
Schorlomite (Slm)	0.00	5.55			
Schorlomite-Al	**10.25**	**10.00**			
Morimotoite (Mrm)	0.63	2.27			
Morimotoite-Mg	**8.33**	**12.13**			
Uvarovite (Uv)	0.03	0.01			
Spessartine (Sps)	0.34	0.00			
Andradite (Adr)	**79.56**	**68.70**			
Calderite	0.53	0.95			
Khoharite	0.32	0.38			
Remainder	0.00	0.00			
Total	99.99	99.99			
Quality index	Superior	Superior			

[a]Electron microprobe data were analyzed using the spreadsheet from Locock (2008), which was also used in calculating the Fe^{2+}/Fe^{3+} and Mn^{2+}/Mn^{3+} amounts using the method of Droop (1987). Two phases were detected by EMPA. However, three phases were observed by HRPXRD (MC9a = phase 1, and MC9b = phase 2). Numbers in bold indicate significant end-members.

The structural models for the Ti-rich andradite sample were refined quite well, as shown by the Rietveld statistics (Table II). The EMPA analyses show that the Ca(X) site occupancy factors (*sofs*) are very close to 1.0, and the refinement values are about 0.94 (Table III). The EMPA *sofs* for the Fe (Y) site are about 0.94, whereas the refinement values vary from about 0.82 to 0.85. The EMPA *sofs* for the Si(Z) site are close to 1.0, and the refinement values vary from about 0.96 to 1.04, so the hydroxyl substitution, $(O_4H_4) \leftrightarrow SiO_4$, is negligible. The *sofs* are compared further in terms of differences between electrons and *sofs* obtained by Rietveld refinement and EMPA (Table III).

TABLE II. HRPXRD data and Rietveld refinement statistics.

	Phase 1	Phase 2	Phase 3
Wt%	46.5(1)	23.9(1)	29.6(1)
a (Å)	12.077 57(2)	12.094 35(2)	12.065 25(1)
Δa (Å)[a]		−0.0168	0.0123
LY[b]	15.61	10.71	5.77
Reduced χ^2	1.183		
R (F^2)[c]	0.0295		
N_{obs}	2096		
λ (Å)	0.413 51(2)		
2θ range	2 to 50°		
Data points	47991		

[a]In thin film theory (Kitamura and Komatsu, 1978), both the strain and birefringence between the substrate and film are proportional to Δa ($a_{substrate} - a_{film}$).
[b]LY is related to strain and these values are quite large compared to a single phase andradite (MC7), where LY = 3.29 (unpublished result).
[c]R (F^2) = overall R-structure factor based on observed and calculated structure amplitudes $=[\sum(F_o^2 - F_c^2)/\sum(F_o^2)]^{1/2}$.

Figure 3 was constructed using average ⟨X–O⟩, Y–O, and Z–O distances that were obtained from single-crystal refinements using cubic space group, $Ia\bar{3}d$, for single-phase garnet samples that may or may not be birefringent (Novak and Meyer, 1970; Novak and Gibbs, 1971; Weber *et al.*, 1975; Munno *et al.*, 1980; Basso *et al.*, 1981, 1983, 1984a, 1984b; Sacerdoti and Passaglia, 1985; Lager *et al.*, 1987a, 1987b, 1989; Smyth *et al.*, 1990; Armbruster *et al.*, 1992, 1998; Geiger *et al.*, 1992; Armbruster and Geiger, 1993; Armbruster, 1995; Peterson *et al.*, 1995; Geiger and Armbruster, 1997; Armbruster *et al.*, 1998; Scordari *et al.*, 1999; Schingaro *et al.*, 2001, 2004; Agrosì *et al.*, 2002; Gramaccioli *et al.*, 2002; Ferro *et al.*, 2003; Chakhmouradian and McCammon, 2005; Adamo *et al.*, 2010). Data for non-cubic, single-phase, single-crystal refinements for birefringent garnet samples are not included in Figure 3 (Takéuchi *et al.*, 1982; Allen and Buseck, 1988; Angel *et al.*, 1989; Kingma and Downs, 1989; Griffen *et al.*, 1992; Nakatsuka *et al.*, 1999a, 1999b; Shtukenberg *et al.*, 2001, 2005; Wildner and Andrut, 2001; Frank-Kamenetskaya *et al.*, 2007). The mean ⟨D–O⟩ distance was calculated using the formula ⟨D–O⟩ = {(Z–O) + (Y–O) +

https://doi.org/10.1017/S0885715613000523 Published online by Cambridge University Press

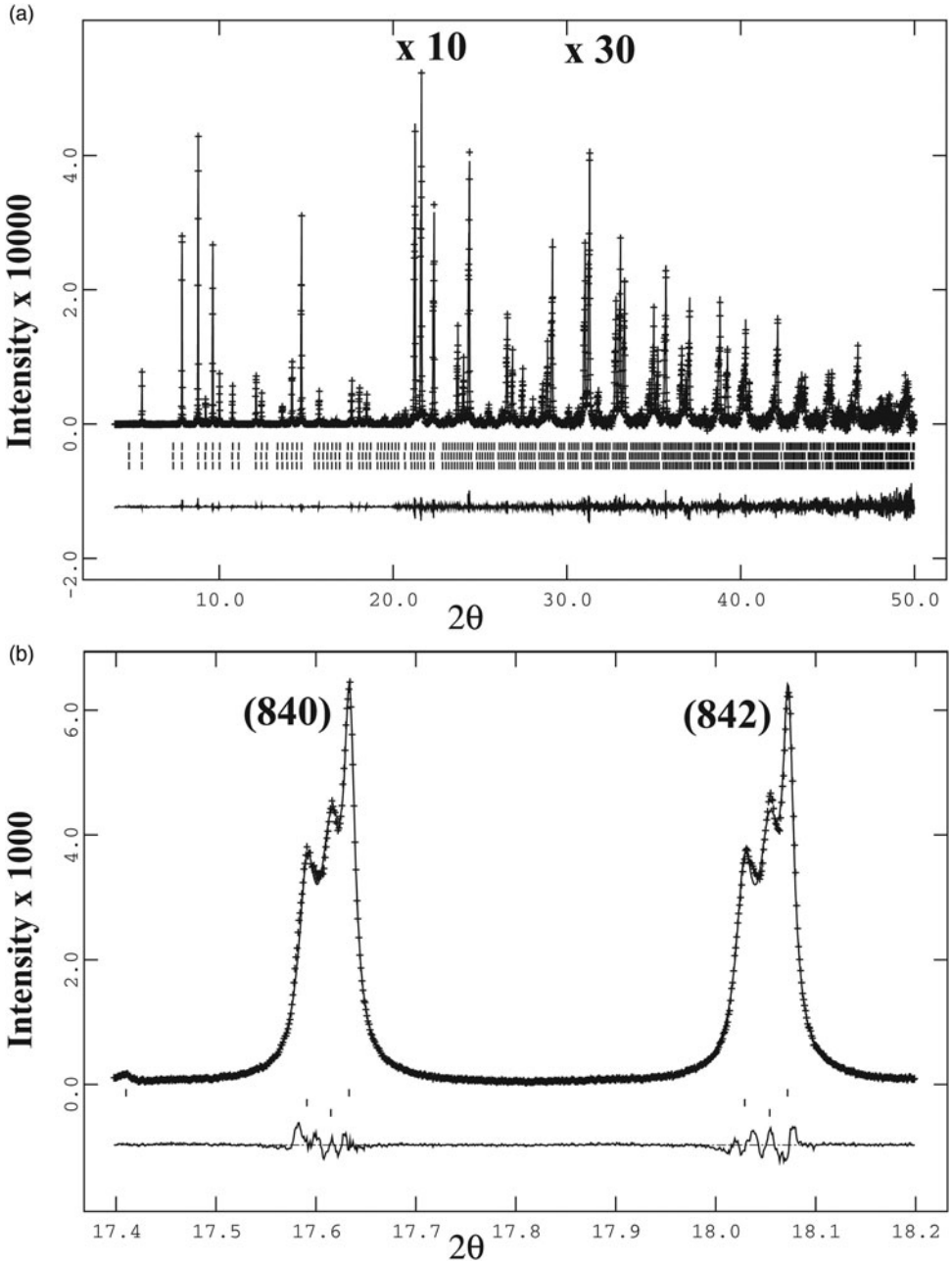

Figure 2. HRPXRD trace for a Ti-rich andradite sample (MC9) from Magnet Cove together with the calculated (continuous line) and observed (crosses) profiles. The difference curve ($I_{obs} - I_{calc}$) is shown at the bottom. The short vertical lines indicate allowed reflection positions. (a) The intensities that are above 20 and 30° 2θ are scaled by factors of ×10 and ×30, respectively, for both the trace and difference curves. (b) The fitted HRPXRD trace showing the reflections (840) and (842). Three cubic phases intergrown in the sample are evident, as indicated by the splitting of the diffraction peaks.

(X–O) + (X′–O)}/4, and it is linear across the entire garnet series (*a* varies from about 11.44 to 12.57 Å). The average ⟨X–O⟩ distance across the garnet series falls on two straight lines that meet at grossular (Grs). The Z–O distance for the anhydrous garnets falls on three straight lines that meet at andradite (Adr) and Ti–Gt, which is a synthetic Ti-rich garnet (Weber *et al.*, 1975). The Y–O distance falls on four straight lines that meet at Grs, Adr, and Ti–Gt. The Y–O variations show the division of the garnet series into four sub-series, as indicated by the dashed vertical lines. For the hydroxy garnets (OH–Gt), the $Y–O_{(OH–Gt)}$ and $Z–O_{(OH–Gt)}$ distances behave differently from other anhydrous garnets, although the behavior of the average ⟨X–O⟩ distance is the same across the series. Other end members of the garnet series shown in Figure 3 are abbreviated using standard notations (Whitney and Evans, 2010). The three phases from this study are very close to the end-member andradite, ideally $Ca_3(Fe_2^{3+})Si_3O_{12}$.

All the bond distances obtained from this study are reasonable and agree with previous results (Table IV; Figure 3). This is not surprising as the single-crystal method samples the dominant phase, but data from possible minor phases are missing. The single-crystal method is an inadequate technique to examine multi-phase samples. The bond distances also compared well with those obtained from the sum of ionic radii (Table IV; Figure 3). The increase in Z–O distance compared to end-member andradite is not the result of $(O_4H_4) \leftrightarrow SiO_4$ substitution, as in hydroxy garnet. Instead, the increase in Z–O is the result of $(Fe^{3+}, Al) \leftrightarrow Si$ substitution

https://doi.org/10.1017/S0885715613000523 Published online by Cambridge University Press

TABLE III. Atom coordinates[a], isotropic displacement parameters, U (Å^2), and *sofs*.

		Phase 1	Phase 2	Phase 3
Ca(X)	*U*	0.0058(2)	0.0055(2)	0.0060(2)
Fe(Y)	*U*	0.0037(1)	0.0029(1)	0.0028(1)
Si(Z)	*U*	0.0045(2)	0.0042(3)	0.0037(2)
O	*x*	0.038 46(7)	0.038 81(9)	0.038 69(7)
	y	0.047 99(7)	0.048 53(8)	0.048 02(7)
	z	0.654 14(7)	0.653 55(9)	0.654 71(7)
	U	0.0115(3)	0.0099(3)	0.0109(3)
Ca(X)	*sof*	0.948(3)	0.953(3)	0.928(3)
Fe(Y)	*sof*	0.848(2)	0.837(2)	0.819(2)
Si(Z)	*sof*	1.000(3)	1.037(3)	0.957(3)
Ca(X)	*EMPA sofs*	1.001(0)	1.001(0)	–
Fe(Y)	*EMPA sofs*	0.953(4)	0.932(7)	–
Si(Z)	*EMPA sofs*	0.996(7)	1.027(10)	–
X[b]	Δ(*sof*)	−0.053	−0.048	–
Y	Δ(*sof*)	−0.105	−0.095	–
Z	Δ(*sof*)	0.004	0.01	–
X[c]	Δ*e*	−1.06	−0.96	–
Y	Δ*e*	−2.73	−2.47	–
Z	Δ*e*	0.056	0.14	–

[a]X at (0, ¼, ⅛) with Ca dominant, Y at (0, 0, 0) with Fe dominant, and Z at (⅜, 0, ¼) with Si dominant.
[b]Δ(*sof*) = *sof* (HRPXRD refinement) − *sof* (EMPA).
[c]Δ*e* = electrons (HRPXRD refinement) − electrons (EMPA).

in the Z site (Table I). Similarly, the decrease in Y–O distance compared to end-member andradite, arises from the replacement of Fe^{3+} (0.645 Å) by smaller Ti^{4+} (0.605 Å). Since the mean ⟨D–O⟩ distance varies as a straight line and the average ⟨X–O⟩ distances by straight lines, for the Ti-andradite region, when Z–O expands, then Y–O contracts (Figure 3).

The crystal structure of the individual phases in andradite can also be rationalized using bond-valence sums (BVS) calculated in valence units (v.u) (Wills and Brown, 1999). For example, for dominant phase-1, the BVS for Ca atom at X site is 2.30 v.u., whereas BVS for Mn and Mg atoms in this site are low. This means that the Ca atom is a bit large for the X site, whereas the Mg atom is too small, so it rattles and gives rise to large displacement parameters, especially in pyrope; these facts are well known. For Ti^{4+} at the Y site, the BVS is 3.60 v.u., whereas for Fe^{3+}, it is 2.89 v.u. The BVS for Si at Z site is 3.75 v.u., which is reasonable because there are some Al and Fe atoms in this site (Table I).

The formation of multi-phase cubic intergrowths may be related to changes in oxygen fugacity (f_{O2}), activity of SiO_2 (a_{SiO2}), etc., as the crystals grow at low temperature that prevents diffusion or homogenization of the cations. Such intergrowths are similar to hetero-epitaxial or epitaxial growths because of the similarity of the structural and chemical parameters in individual cubic phases. Slight structural differences between the cubic phases give rise to structural mismatch that result in strain and optical anisotropy. A measure of strain can be obtained from the LY profile term in GSAS refinement. For a single-phase cubic garnet, the LY value is small compared to those for the multi-phase andradite, which has larger LY values, indicating larger strain (Table II).

Garnet-group minerals are important as they occur over a range of pressures, temperatures, and chemical compositions. They are common in metamorphic rocks and in xenoliths derived from the Earth's mantle. It is important to know the

TABLE IV. Selected distances (Å) in Ti-rich andradite (MC9).

		Phase 1	Phase 2	Phase 3
Z–O (Å)	x4	1.6639(9)	1.671(1)	1.6559(9)
Y–O	x6	2.0043(9)	2.003(1)	2.0095(9)
X–O	x4	2.3609(8)	2.373(1)	2.3575(8)
X–O′	x4	2.5085(9)	2.505(1)	2.5070(8)
⟨X–O⟩	[8]	2.4347	2.439	2.4323
⟨D–O⟩[a]		2.1344	2.138	2.1325
Radii ∑				
Z–O (Å)		1.649	1.657	–
Y–O		2.022	2.022	–
⟨X–O⟩		2.439	2.438	–
⟨D–O⟩		2.137	2.139	–

These distances are shown in Figure 3 for comparison with published data. For the calculated radii sum distances, radii from Shannon (1976) were used (X site: Mn^{2+} = 0.96, Mg = 0.89 Å; Y site: Ti^{4+} = 0.605, Al = 0.535, Cr^{3+} = 0.615, Fe^{2+} = 0.78, Fe^{3+} = 0.645, Mn^{3+} = 0.645, Mg = 0.72 Å; Z site: Si = 0.26, Al = 0.39, Fe^{3+} = 0.49 Å; O = 1.38 Å). Ca = 1.06 Å instead of 1.12 Å from Shannon (1976); this gives more realistic ⟨X–O⟩ distances.
[a]⟨D–O⟩ = {(Z–O) + (Y–O) + (X–O) + (X′–O)}/4.

https://doi.org/10.1017/S0885715613000523 Published online by Cambridge University Press

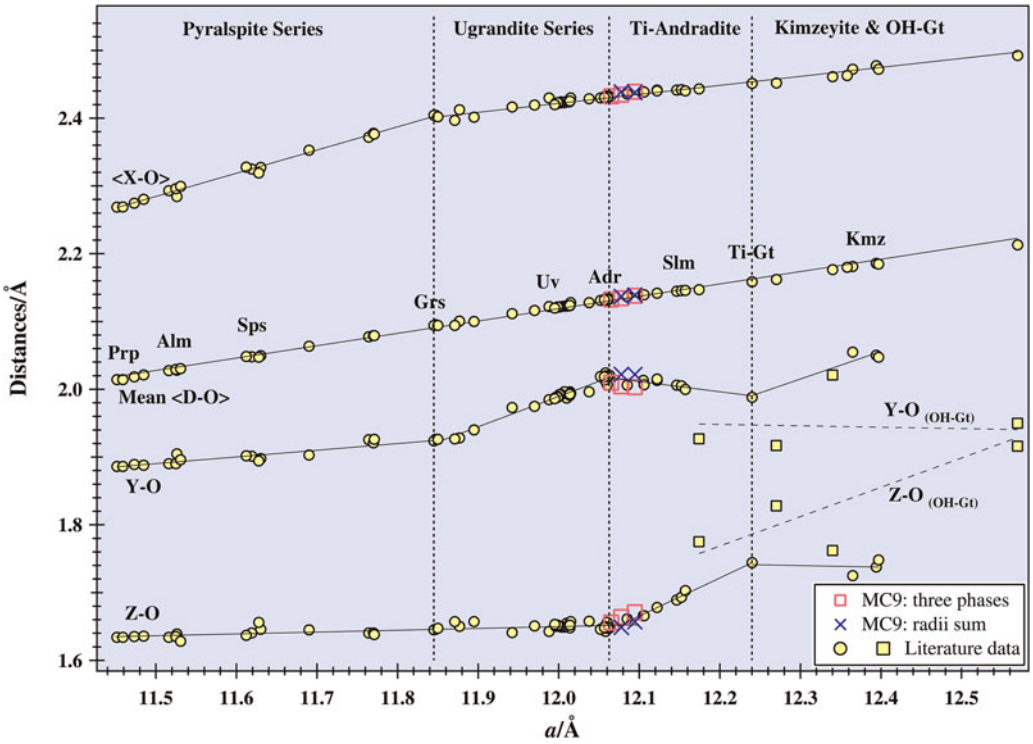

Figure 3. (Color online) Structural variations across the silicate garnet series. The Y–O, Z–O, and average ⟨X–O⟩ distances vary linearly with the *a* unit-cell parameter in different parts of the series. The mean ⟨D–O⟩ distance varies linearly with the *a* parameter across the entire series. The linear lines are based on literature data (see text). Standard abbreviations are used for garnet end members, including slm = schorlomite and kmz = kimzeyite. Data from this study are also shown.

structural effects that arise from cation substitutions so as to interpret the complex (ideal or non-ideal) thermodynamic behavior observed in garnet solid solutions (Ganguly *et al.*, 1993), and their petrogenetic significances. Most geothermometers and geobarometers involve garnet as one of the phases (Ganguly *et al.*, 1993).

Majorite garnet, $(Mg,Fe)SiO_3$, is considered to be a major constituent of the Earth's transition zone between the 400- and 670-km discontinuities (Ringwood, 1967; Akaogi and Akimoto, 1977; Liu, 1977). Anisotropic $MgSiO_3$, that is, $\{Mg_3\}(MgSi)[Si_3O_{12}]$, garnet accounts for a large fraction of the Earth's upper mantle above the 670-km discontinuity (Ito and Takahashi, 1987), and was reported to be birefringent with tetragonal symmetry (Kato and Kumazawa, 1985; Sawamoto, 1987; Angel *et al.*, 1989; Parise *et al.*, 1996; Nakatsuka *et al.*, 1999a, 1999b). High-pressure synthesis has produced ABO_3 tetragonal phases such as $CaGeO_3$, $CdGeO_3$ (Prewitt and Sleight, 1969; Nakatsuka *et al.*, 2005), and $MnSiO_3$ (Fujino *et al.*, 1986), in which equal numbers of A and B atoms are ordered on the Y site. If cation order and cubic symmetry reduction occur for birefringent ABO_3 garnet, then the thermodynamic properties of $MgSiO_3$ garnet in the mantle will change significantly, and that has important geophysical consequences. The configurational entropy of an ordered tetragonal $MgSiO_3$ garnet would be reduced relative to a disordered cubic phase, and gives rise to a reduction in enthalpy. Therefore, possible cubic to tetragonal phase transition in $MgSiO_3$ garnet and the associated cation ordering on the Y site are of considerable interest in terms of thermodynamic effects and seismic velocities in the transition zone. Contrary to the structural results obtained so far on birefringent ABO_3 garnet samples that undergo a cubic to tetragonal transition, the results from this study suggest that they may be cubic and may occur as a mixture of cubic phases, hence further work remains to be done on ABO_3 garnet samples. Birefringence in natural samples disappears at about 800 °C and may or may not reappear on cooling (Prewitt and Sleight, 1969).

Natural garnet such as uvarovite, $\{Ca_3\}[Cr_2^{3+}](Si_3)O_{12}$; grossular, $\{Ca_3\}[Al_2](Si_3)O_{12}$; andradite, $\{Ca_3\}[Fe_2^{3+}](Si_3)O_{12}$; spessartine, $\{Mn_3^{2+}\}[Al_2](Si_3)O_{12}$; almandine, $\{Fe_3^{2+}\}[Al_2](Si_3)O_{12}$; and hydrogarnets can be birefringent and consist of a mixture of two or three cubic phases, whereas other garnets such as pyrope, $\{Mg_3\}[Al_2](Si_3)O_{12}$, is isotropic, if they occur as a single cubic phase (unpublished results). The hydrogarnet series between grossular, $\{Ca_3\}[Al_2](SiO_4)_3$ – $\{Ca_3\}[Al_2](O_4H_4)_3$, (Si-free katoite), is known as "hydrogrossular", and between andradite $\{Ca_3\}[Fe_2^{3+}](SiO_4)_3$ – $\{Ca_3\}[Fe_2^{3+}](O_4H_4)_3$, is known as "hydroandradite". Unusual and elongated atomic displacement parameters along the "Si-O" bond for the O atoms in hydrogarnets are usually modeled by split O-atom positions (e.g., Lager *et al.*, 1987b; Armbruster and Lager, 1989; Ferro *et al.*, 2003), but they are the result of multiple cubic phases (unpublished results). Similar unusual O-atom features were also observed for the Ice River morimotoite (Peterson *et al.*, 1995), and are also the result of multiple phases (unpublished results). The crystal structure of birefringent andradite samples was recently discussed by Antao and Klincker (2013) and Antao (2013); the crystal structure of other birefringent garnets will be published elsewhere. Birefringent garnet consists of a mixture of two or more cubic phases. This mixture causes strain that arises from

https://doi.org/10.1017/S0885715613000523 Published online by Cambridge University Press

structural mismatch and makes the garnet birefringent. A long standing problem on birefringent garnets now appears to be solved.

ACKNOWLEDGEMENTS

I thank the two anonymous reviewers for their comments. I also thank J. Nicholls for his comments on an earlier draft of this manuscript. J. Michael Howard is thanked for providing a suite of Ti-rich andradite samples from Magnet Cove, Hot Spring County, Arkansas. R. Marr is thanked for help with the EMPA data collection. The HRPXRD data were collected at the X-ray Operations and Research beamline 11-BM, Advanced Photon Source (APS), Argonne National Laboratory (ANL). Use of the APS was supported by the U.S. Dept. of Energy, Office of Science, Office of Basic Energy Sciences, under Contract No. DE-AC02-06CH11357. This work was supported with an NSERC Discovery Grant and an Alberta Ingenuity Award.

Adamo, I., Gatta, G. D., Rotitoti, N., Diella, V., and Pavese, A. (**2010**). "Green andradite stones: gemological and mineralogical characterisation," Eur. J. Miner. **23**, 91–100.

Agrosì, G., Schingaro, E., Pedrazzi, G., Scandale, E., and Scordari, R. (**2002**). "A crystal chemical insight into sector zoning of a titanian andradite ("melanite") crystal," Eur. J. Miner. **14**, 785–794.

Akaogi, M. and Akimoto, S. (**1977**). "Pyroxene-garnet solid-solution equilibria in the systems $Mg_4Si_40_{12}$-$Mg_3Al_2Si_3O_{12}$ and $Fe_4Si_4O_{12}$-$Fe_3Al_2Si_3O_{12}$ at high pressures and temperatures," Phys. Earth Planet. Interiors **15**, 90–106.

Akizuki, M. (**1984**). "Origin of optical variations in grossular-andradite garnet," Am. Miner. **66**, 403–409.

Akizuki, M., Takéuchi, Y., Terada, T., and Kudoh, Y. (**1998**). "Sectoral texture of a cubo-dodecahedral garnet in grandite," Neues Jahrbuch für Mineralogie, Monatshefte **12**, 565–576.

Allen, F. M. and Buseck, P. R. (**1988**). "XRD, FTIR, and TEM studies of optically anisotropic grossular garnets," Am. Miner. **73**, 568–584.

Angel, R., Finger, L. W., Hazen, R. M., Kanzaki, M., Weidner, D. J., Liebermann, R. C., and Veblen, D. R. (**1989**). "Structure and twinning of single-crystal $MgSiO_3$ garnet synthesized at 17 GPa and 1800 °C," Am. Miner. **74**, 509–512.

Antao, S. M. (**2013**). "Three cubic phases intergrown in a birefringent andradite-grossular garnet and their implications," *Phys. Chem. Miner.* DOI: 10.1007/s00269-013-0606-4.

Antao, S. M. and Klincker, A. M. (**2013**). "Origin of birefringence in andradite from Arizona, Madagascar, and Iran," Phys. Chem. Miner. **40**, 575–586.

Antao, S. M., Hassan, I., Wang, J., Lee, P. L., and Toby, B. H. (**2008**). "State-of-the-art high-resolution powder X-ray diffraction (HRPXRD) illustrated with Rietveld structure refinement of quartz, sodalite, tremolite, and meionite," Can. Miner. **46**, 1501–1509.

Antao, S. M., Klincker, A. M., and Round, S. A. (**2013a**). "Origin of birefringence in common silicate garnet: intergrowth of different cubic phases," Am. Geophys. Union Conference, Cancun, Mexico, 14–17 May, 2013.

Antao, S. M., Klincker, A. M., and Round, S. A. (**2013b**). "Some garnets are cubic and birefringent, why?," Conference, Hawaii, USA, 20–24 July, 2013.

Armbruster, T. (**1995**). "Structure refinement of hydrous andradite, $Ca_3Fe_{1.54}Mn_{0.02}Al_{0.26}(SiO_4)_{1.65}(O_4H_4)_{1.35}$, from the Wessels mine, Kalahari manganese field, South Africa," Eur. J. Miner. **7**, 1221–1225.

Armbruster, T. and Geiger, C. A. (**1993**). "Andradite crystal chemistry, dynamic x-site disorder and structural strain in silicate garnets," Eur. J. Miner. **5**, 59–71.

Armbruster, T. and Lager, G. A. (**1989**). "Oxygen disorder and the hydrogen position in garnet-hydrogarnet solid-solutions," Eur. J. Miner. **1**, 363–369.

Armbruster, T., Geiger, C. A., and Lager, G. A. (**1992**). "Single crystal X-ray structure study of synthetic pyrope-almandine garnets at 100 and 293 K," Am. Miner. **77**, 518–527.

Armbruster, T., Birrer, J., Libowitzky, E., and Beran, A. (**1998**). "Crystal chemistry of Ti-bearing andradites," Eur. J. Miner. **10**, 907–921.

Badar, M. A., Akizuki, M., and Hussain, S. (**2010**). "Optical anomaly in iridescent andradite from the Sierra Madre mountains, Sonora, Mexico," Can. Miner. **48**, 1195–1203.

Badar, M. A., Niaz, S., Hussain, S., and Akizuki, M. (**2013**). "Lamellar texture and optical anomaly in andradite from the Kamaishi mine, Japan," Eur. J. Miner. **25**, 53–60.

Basso, R., Dellagiusta, A., and Zefiro, L. (**1981**). "A crystal chemical study of a Ti-containing hydrogarnet," Neues Jahrbuch Fur Mineralogie-Monatshefte **5**, 230–236.

Basso, R., Dellagiusta, A., and Zefiro, L. (**1983**). "Crystal-structure refinement of plazolite - a highly hydrated hatural hydrogrossular," Neues Jahrbuch Fur Mineralogie-Monatshefte **6**, 251–258.

Basso, R., Cimmino, F., and Messiga, B. (**1984a**). "Crystal-chemistry of hydrogarnets from three different microstructural sites of a basaltic metarodingite from the Voltri-Massif (Western Liguria, Italy)," Neues Jahrbuch Fur Mineralogie-Abhandlungen **148**, 246–258.

Basso, R., Cimmino, F., and Messiga, B. (**1984b**). "Crystal chemical and petrological study of hydrogarnets from a Fe-gabbro metarodingite (Gruppo Di Voltri, Western Liguria, Italy)," Neues Jahrbuch Fur Mineralogie-Abhandlungen **150**, 247–258.

Bertaut, F. and Forrat, F. (**1956**). "Structures des ferrites ferrimagnétiques des terres rare," C. R. Acad. Sci. **243**, 382–384.

Blanc, Y. and Maisonneuve, J. (**1973**). "Sur la biréfringence des grenats calciques," Bull. Soc. Franç. Minér. Cristallogr. **96**, 320–321.

Brauns, R. (**1891**). *Die optischen Anomalien der Kristalle*. Preisschr. (Jablonowski Ges., Leipzig, Germany).

Brown, D. and Mason, R. A. (**1994**). "An occurrence of sectored birefringence in almandine from the Gangon terrane, Labrador," Can. Miner. **32**, 105–110.

Chakhmouradian, A. R. and McCammon, C. A. (**2005**). "Schorlomite: a discussion of the crystal chemistry, formula, and inter-species boundaries," Phys. Chem. Miner. **32**, 277–289.

Chase, A. B. and Lefever, R. A. (**1960**). "Birefringence of synthetic garnets," Am. Miner. **45**, 1126–1129.

Droop, G. T. R. (**1987**). "A general equation for estimating Fe^{3+} concentrations in ferromagnesian silicates and oxides from microprobe analyses, using stoichiometric criteria," Miner. Mag. **51**, 431–435.

Ferro, O., Galli, E., Papp, G., Quartieri, S., Szakall, S., and Vezzalini, G. (**2003**). "A new occurrence of katoite and re-examination of the hydrogrossular group," Eur. J. Miner. **15**, 419–426.

Foord, E. E. and Mills, B. A. (**1978**). "Biaxiality in "isometric" and "dimetric" crystals," Am. Miner. **63**, 316–325.

Frank-Kamenetskaya, O. V., Rozhdestvenskaya, L. V., Shtukenberg, A. G., Bannova, I. I., and Skalkina, Y. A. (**2007**). "Dissymmetrization of crystal structures of grossular-andradite garnets $Ca_3(Al, Fe)_2(SiO_4)_3$," Struct. Chem. **18**, 493–503.

Fujino, K., Momoi, H., Sawamoto, H., and Kumazawa, M. (**1986**). "Crystal structure and chemistry of $MnSiO_3$ tetragonal garnet," Am. Miner. **71**, 781–785.

Ganguly, J., Cheng, W., and O'Neill, H. S. C. (**1993**). "Syntheses, volume, and structural changes of garnets in the pyrope-grossular join: implications for stability and mixing properties," Am. Miner. **78**, 583–593.

Geiger, C. A. and Armbruster, T. (**1997**). "$Mn_3Al_2Si_3O_{12}$ spessartine and $Ca_3Al_2Si_3O_{12}$ grossular garnet: structural dynamic and thermodynamic properties," Am. Miner. **82**, 740–747.

Geiger, C. A., Armbruster, T., Lager, G. A., Jiang, K., Lottermoser, W., and Amthauer, G. (**1992**). "A combined temperature dependent ^{57}Fe Mössbauer and single crystal X-ray diffraction study of synthetic lmandine: evidence for the Gol'danskii-Karyagin effect," Phys. Chem. Miner. **19**, 121–126.

Geller, S. (**1967**). "Crystal chemistry of garnets," Z. Kristal **125**, 1–47.

Geller, S. and Gilleo, M. A. (**1957**). "Structure and ferrimagnetism of yttrium and rare earth iron garnets," Acta Crystallogr. **10**, 239.

Geusic, J. E., Marcos, H. M., and Van Uitert, L. G. (**1964**). "Laser oscillations in Nd-doped yttrium aluminum, yttrium gallium and gadolinium garnets," Appl. Phys. Lett. **4**, 182–184.

Gramaccioli, C. M., Pilati, T., and Demartin, F. (**2002**). "Atomic displacement parameters for spessartine $Mn_3Al_2Si_3O_{12}$ and their lattice-dynamical interpretation," Acta Crystallogr. **B58**, 965–969.

Griffen, D. T., Hatch, D. M., Phillips, W. R., and Kulaksiz, S. (**1992**). "Crystal chemistry and symmetry of a birefringent tetragonal pyralspite$_{75}$-grandite$_{25}$ garnet," Am. Miner. **77**, 399–406.

Hatch, D. M. and Ghose, S. (**1989**). "Symmetry analysis of the phase transition and twinning in $MgSiO_3$ garnet: implications to mantle mineralogy," Am. Miner. **74**, 1221–1224.

Henmi, C., Kusachi, I., and Henmi, K. (**1995**). "Morimotoite, $Ca_3TiFe^{2+}Si_3O_{12}$, a new titanian garnet from Fuka, Okayama Prefecture, Japan," Miner. Mag. **59**, 115–120.

Hofmeister, A. M., Schaal, R. B., Campbell, K. R., Berry, S. L., and Fagan, T. J. (**1998**). "Prevalence and origin of birefringence in 48 garnets from the pyrope-almandine- grossularite-spessartine quaternary," Am. Miner. **83**, 1293–1301.

Ingerson, E. and Barksdale, J. D. (**1943**). "Iridescent garnet from the Adelaide mining district, Nevada," Am. Miner. **28**, 303–312.

Ito, E. and Takahashi, E. (**1987**). "Ultrahigh pressure phase transformations and the constitution of the deep mantle," in *High Pressure Research in Mineral Physics: A Volume in Honor of Syun-iti Akimoto, Geophysical Monograph*, edited by M. H. Manghnani and Y. Syono, AGU, Washington, D.C. Vol. **39**, pp. 221–229.

Kato, T. and Kumazawa, M. (**1985**). "Garnet phase of $MgSiO_3$ filling the pyroxene-ilmenite gap at very high temperature," Nature **316**, 803–805.

Kingma, K. J. and Downs, J. W. (**1989**). "Crystal-structure analysis of a birefringent andradite," Am. Miner. **74**, 1307–1316.

Kitamura, K. and Komatsu, H. (**1978**). "Optical anisotropy associated with growth striation of yttrium garnet, $Y_3(Al,Fe)_5O_{12}$," Kristallogr. Tech. **13**, 811–816.

Lager, G. A., Rossman, G. R., Rotella, F. J., and Schultz, A. J. (**1987a**). "Neutron-diffraction structure of a low-water grossular at 20 K," Am. Miner. **72**, 766–768.

Lager, G. A., Armbruster, T., and Faber, J. (**1987b**). "Neutron and X-ray-diffraction study of hydrogarnet $Ca_3Al_2(O_4H_4)_3$," Am. Miner. **72**, 756–765.

Lager, G. A., Armbruster, T., Rotella, F. J., and Rossman, G. R. (**1989**). "OH substitution in garnets: X-ray and neutron diffraction, infrared, and geometric-modeling studies," Am. Miner. **74**, 840–851.

Larson, A. C. and Von Dreele, R. B. (**2000**). *General Structure Analysis System (GSAS)* (Report LAUR 86-748). Los Alamos National Laboratory.

Lee, P. L., Shu, D., Ramanathan, M., Preissner, C., Wang, J., Beno, M. A., Von Dreele, R. B., Ribaud, L., Kurtz, C., Antao, S. M., Jiao, X., and Toby, B. H. (**2008**). "A twelve-analyzer detector system for high-resolution powder diffraction," J. Synchrotron Radiat. **15**, 427–432.

Lessing, P. and Standish, R. P. (**1973**). "Zoned garnet from Crested Butte, Colorado," Am. Miner. **58**, 840–842.

Liu, L. (**1977**). "The system enstatite-pyrope at high pressures and temperatures and the mineralogy of the Earth's mantle," Earth Planet. Sci. Lett. **36**, 237–245.

Locock, A. J. (**2008**). "An excel spreadsheet to recast analyses of garnet into end-member components, and a synopsis of the crystal chemistry of natural silicate garnets," Comput. Geosci. **34**, 1769–1780.

Munno, R., Rossi, G., and Tadini, C. (**1980**). "Crystal chemistry of kimzeyite from Stromboli, Aeolian Islands, Italy," Am. Miner. **65**, 188–191.

Nakatsuka, A., Yoshiasa, A., Yamanaka, T., Ohtaka, O., Katsura, T., and Ito, E. (**1999a**). "Symmetry change of majorite solid-solution in the system $Mg_3Al_2Si_3O_{12}$-$MgSiO_3$," Am. Miner. **84**, 1135–1143.

Nakatsuka, A., Yoshiasa, A., Yamanaka, T., and Ito, E. (**1999b**). "Structure refinement of a birefringent Cr-bearing majorite $Mg_3(Mg_{0.34}Si_{0.34}Al_{0.18}Cr_{0.14})_2Si_3O_{12}$," Am. Miner. **84**, 199–202.

Nakatsuka, A., Chaya, H., and Yoshiasa, A. (**2005**). "Crystal structure of single-crystal $CaGeO_3$ tetragonal garnet synthesized at 3 GPa and 1000 °C," Am. Miner. **90**, 755–757.

Novak, G. A. and Gibbs, G. V. (**1971**). "The crystal chemistry of the silicate garnets," Am. Miner. **56**, 1769–1780.

Novak, G. A. and Meyer, H. O. A. (**1970**). "Refinement of the crystal structure of a chrome pyrope garnet: an inclusion in natural diamond," Am. Miner. **55**, 2124–2127.

Parise, J. B., Wang, Y., Gwanmesia, G. D., Zhang, J., Sinelnikov, Y., Chmielowski, J., Weidner, D. J., and Liebermann, R. C. (**1996**). "The symmetry of garnets on the pyrope ($Mg_3Al_2Si_3O_{12}$) – majorite ($MgSiO_3$) join," Geophys. Res. Lett. **23**, 3799–3802.

Peterson, R. C., Locock, A. J., and Luth, R. W. (**1995**). "Positional disorder of oxygen in garnet: the crystal-structure refinement of schorlomite," Can. Miner. **33**, 627–631.

Prewitt, C. T. and Sleight, A. W. (**1969**). "Garnet-like structures of high-pressure cadmium germanate and calcium germanate," Science **163**, 386–387.

Rietveld, H. M. (**1969**). "A profile refinement method for nuclear and magnetic structures," J. Appl. Crystallogr. **2**, 65–71.

Ringwood, A. E. (**1967**). "The pyroxene-garnet transformation in the Earth's mantle," Earth Planet. Sci. Lett. **2**, 255–263.

Rossman, G. R. and Aines, R. D. (**1986**). "Spectroscopy of a birefringent grossular from Asbestos, Quebec, Canada," Am. Miner. **71**, 779–780.

Sacerdoti, M. and Passaglia, E. (**1985**). "The crystal structure of katoite and implications within the hydrogrossular group of minerals," Bull. Miner. **108**, 1–8.

Sawamoto, H. (**1987**). "Phase diagram of $MgSiO_3$ at pressures up to 24 GPa and temperatures up to 2200 °C: phase stability and properties of tetragonal garnet," in *High Pressure Research in Mineral Physics: A Volume in Honor of Syun-iti Akimoto, Geophysical Monograph*, edited by M. H. Manghnani and Y. Syono, AGU, Washington, D.C. Vol. **39**, 209–219.

Schingaro, E., Scordari, F., Capitanio, F., Parodi, G., Smith, D. C., and Mottana, A. (**2001**). "Crystal chemistry of kimzeyite from Anguillara, Mt. Sabatini, Italy," Eur. J. Miner. **13**, 749–759.

Schingaro, E., Scordari, F., Pedrazzi, G., and Malitesta, C. (**2004**). "Ti and Fe speciation by X-ray photoelectron spectroscopy (XPS) and mössbauer spectroscopy for a full crystal chemical characterisation of Ti-garnets from Colli Albani (Italy)," Ann. Chim. **94**, 185–196.

Scordari, F., Schingaro, E., and Pedrazzi, G. (**1999**). "Crystal chemistry of melanites from Mt. Vulture (Southern Italy)," Eur. J. Miner. **11**, 855–869.

Shannon, R. D. (**1976**). "Revised effective ionic radii and systematic studies of interatomic distances in halides and chalcogenides," Acta Crystallogr. Sect. A: Cryst. Phys., Diffr., Theor. Gen. Crystallogr. **32**, 751–767.

Shtukenberg, A. G., Punin, Y. O., Frank-Kamenetskaya, O. V., Kovalev, O. G., and Sokolov, P. B. (**2001**). "On the origin of anomalous birefringence in grandite garnets," Miner. Mag. **65**, 445–459.

Shtukenberg, A. G., Popov, D. Y., and Punin, Y. O. (**2005**). "Growth ordering and anomalous birefringence in ugrandite garnets," Miner. Mag. **69**, 537–550.

Smyth, J. R., Madel, R. E., McCormick, T. C., Munoz, J. L., and Rossman, G. R. (**1990**). "Crystal-structure refinement of a F-bearing spessartine garnet," Am. Miner. **75**, 314–318.

Takéuchi, Y., Haga, N., Umizu, S., and Sato, G. (**1982**). "The derivative structure of silicate garnets in grandite," Z. Kristallogr. **158**, 53–99.

Toby, B. H. (**2001**). "EXPGUI, a graphical user interface for GSAS," J. Appl. Crystallogr. **34**, 210–213.

Wang, J., Toby, B. H., Lee, P. L., Ribaud, L., Antao, S. M., Kurtz, C., Ramanathan, M., Von Dreele, R. B., and Beno, M. A. (**2008**). "A dedicated powder diffraction beamline at the advanced photon source: commissioning and early operational results," Rev. Sci. Instrum. **79**, 085105.

Weber, H. P., Virgo, D., and Huggins, F. E. (**1975**). "A neutron-diffraction and ^{57}Fe Mössbauer study of a synthetic Ti-rich garnet," Carnegie Inst. Wash. Year Book **74**, 575–579.

Whitney, D. L. and Evans, B. W. (**2010**). "Abbreviations for names of rock-forming minerals," Am. Miner. **95**, 185–187.

Wildner, M. and Andrut, M. (**2001**). "The crystal chemistry of birefringent natural uvarovites: part II. Single-crystal X-ray structures," Am. Miner. **86**, 1231–1251.

Wills, A. S. and Brown, I. D. (**1999**). VaList. CEA, France. This is a freely available computer program.